Frustrated pulse-area quantization in accelerated superradiant atom-cavity systems

C. Greiner, B. Boggs, and T. W. Mossberg

Oregon Center for Optics and Department of Physics, University of Oregon, Eugene, Oregon 97403, USA
(Received 26 March 2002; published 19 June 2003)

In self-induced transparency (SIT), as described by the McCall-Hahn area theorem, the area of an optical pulse is modified as it propagates through a resonant absorbing medium, and in the limit of high optical thickness evolves to certain discrete (quantized) output values. We investigate the area evolution experienced by an optical pulse when interacting with an absorbing medium contained within a cavity. In the system studied, the intracavity medium is weakly attenuating on a single-pass basis, but the atom-cavity system's effective optical thickness as viewed from input to output port is generally quite large. Interestingly, at the low end of effective optical thickness we find that the cavity system generates pulse-area evolution closely mirroring that seen in the SIT system, i.e., output pulse areas evolve toward stable values as the effective optical thickness increases. However, when the effective optical thickness increases to certain triggering levels, the output pulse area is seen to drop abruptly toward zero. Our theoretical predictions are experimentally probed using cavity-contained cryogenically coherence-stabilized Tm^{3+} ions.

The concept of optical pulse area is important since it provides a means of measuring the effect of a general optical field on the internal state of a microscopic quantum system. In a sense, pulse area is a macroscopic handle on the microscopic world. Consequently, systems that provide for the control of optical pulse area are of interest as tools in the manipulation of quantum systems as is necessary in so many areas of current interest such as quantum computing, coherent control, creation of entangled quantum states, etc.

Self-induced transparency (SIT) [1–5] and the McCall-Hahn area theorem [1] provide such a means of achieving control over optical pulse area. On passing through an optically thick absorbing two-level medium, optical pulses emerge as solitons having discrete stabilized areas [1,6,7]. Input pulses over continuous area ranges are mapped to these specific well-defined output values. While SIT was originally predicted for two-level media, similar behavior has been shown to occur in two-pulse propagation through *V*-type three-level media [8]. Control not only over output pulse area, but also output direction was predicted for a dual-waveguide coupler doped with two-level atoms [9]. Note that the two-level area theorem was recently rederived so as to allow for inclusion of pulse chirping [10].

In the present paper, we explore the pulse-area evolution and control features of a weakly absorbing two-level medium contained within an optical cavity. Previously, we demonstrated [11] that this system supports strong superradiance [12–14] under conditions close to those originally envisioned by Dicke in his seminal 1954 superradiance paper [15] and can through its coherent emission significantly modify the area of optical pulses incident on and passing it [16]. For homogenous atomic broadening, the cavity +absorber system was seen to map continuous ranges of input pulse areas to discrete (quantized) output values. For inhomogeneously broadened atoms, ranges of output pulse areas occurred that had gaps in their allowed values [16]. In the former instance, the cavity+absorber system forms the basis for devices that stabilize optical pulse areas to specific values despite input variations. An optical source intrinsi-

cally stabilized to pulse area rather than power or frequency is unusual and potentially useful.

In the present work, we explore the variation of intracavity and output pulse area, as the cavity's effective optical thickness is varied and the input pulse area is held constant. The cavity's effective optical thickness as viewed from input to output port is determined by mirror reflectivities and intracavity absorption and exceeds the medium's single-pass absorption. We find that for values of effective optical thickness below critical levels the pulse area in the cavity system evolves in a manner quite similar to that found in a SIT system. At high effective optical thickness, however, area evolution found in the cavity system is dramatically differently from SIT and the cavity output pulse area is seen to drop abruptly toward zero. Differences between SIT and cavity area behavior at higher effective optical thickness derive from the fact that area evolution in self-induced transparency is inherently a propagational effect, where input pulses continually interact with new atoms, whereas in the cavity +absorber system area evolution derives from interactions with a fixed set of atoms. We experimentally probe the predicted variation of intracavity area with effective optical thickness providing one of the first demonstrations of McCall-Hahn-like input-output area mapping and the signature discontinuities special to the cavity system.

Consider the atom-cavity system shown in Fig. 1(a), which consists of an ensemble of initially unexcited two-level atoms located inside a unidirectional four-mirror ring cavity. The absorptive atomic transition is inhomogeneously broadened with a Gaussian line shape of linewidth $\Delta\nu_{inhom}$ (full width at half maximum) and a Beer's law line center absorption coefficient α. Two of the cavity mirrors are partial with power reflectivity R. The empty-cavity photon lifetime is denoted by τ_c. A plane-wave input pulse with a duration τ_{in} impinges on the cavity entrance mirror at time $t=0$. We assume $\tau_{in} \gg \tau_c$, $1/\Delta\nu_{inhom}$. The center frequencies of the input field, atomic absorption line, and cavity resonance coincide. Due to atomic emission, the field within the cavity may differ substantially from the input field. We refer to the modified field within the cavity as the intracavity field. A
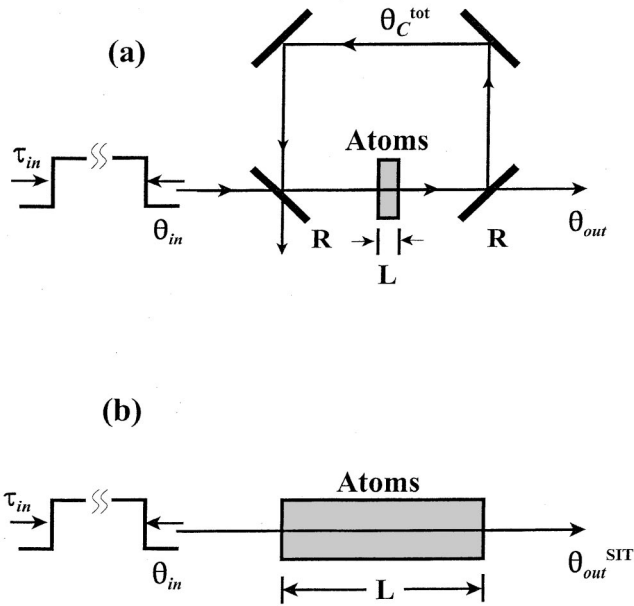
FIG. 1. (a) Ring-cavity model system. R, mirror reflectivity; θ_C^{tot}, θ_{in}, and θ_{out} areas of the intracavity and cavity-external input and output fields. (b) SIT system; τ_{in}, input-pulse duration; L, medium length.

portion of the intracavity field emerges from the cavity, as shown in Fig. 1(a) to form the output field.

The area of an optical pulse is defined as [3]

$$\theta = \frac{p}{\hbar} \int_{-\infty}^{\infty} E(t') dt', \tag{1}$$

where p is the transition dipole moment and $\hbar$ Planck's constant. The pulse areas of the input, intracavity, and output fields are denoted by θ_{in}, θ_C^{tot}, and θ_{out}, respectively. The intracavity pulse area accrued up to a specific time, $t < \infty$, is denoted by $\theta_C(t)$. Note that $\theta_C^{\text{tot}} = \theta_C(t \rightarrow \infty)$ defines the final quantum state of the line center atoms in the inhomogenously broadened absorption line. We further define $\theta_C^0 = \theta_{\text{in}}(1-R)^{-1/2}$ as the intracavity area in the absence of cavity-internal absorbers. In all calculations, cavity loss mechanisms other than mirror transmission are ignored.

Figure 1(b) is a schematic of the SIT system. As for the cavity system, the atoms are assumed to be inhomogeneously broadened with linewidth $\Delta \nu_{\text{inhom}} \gg 1/\tau_{\text{in}}$. The output area of the SIT system is denoted by $\theta_{\text{out}}^{\text{SIT}}$. In all calculations we ignore homogeneous atomic decoherence.

The weak-signal intensity transmission for the SIT system is given by Beer's law

$$\frac{I_{\text{out}}}{I_{\text{in}}} = e^{-\alpha L}, \tag{2}$$

where $I_{\text{out}}(I_{\text{in}})$ is the output (input) intensity and the product of α and medium length L is referred to as the medium's optical thickness. For the cavity system,

$$\frac{I_{\text{out}}}{I_{\text{in}}} = e^{-f(\eta)} \tag{3}$$

and the *effective* optical thickness $f(\eta)$ is given by

$$f(\eta) \approx 2 \ln\left[\frac{\eta}{2} + 1\right]. \tag{4}$$

Here, $\eta = \alpha L/(1-R)$ and the relationship is valid for weak intracavity absorbers ($\alpha L \ll 1$). Note that for $\alpha L \ll 1 - R$, $f(\eta) \approx \eta$. In this limit, the total energy absorbed by the sample in the cavity is $1/(1-R)$ times that absorbed in single-pass transmission.

For the SIT system, the McCall-Hahn area theorem describes the pulse area evolution for input pulses of general areas [1]. For the cavity system, we derive the following analytic relationship between η and θ_C^{tot},

$$\theta_C^0 = \theta_C^{\text{tot}}(\eta) + \frac{\eta}{2} \sin[\theta_C^{\text{tot}}(\eta)]. \tag{5}$$

Equation (5) derives from the differential equation for the intracavity field, which includes all field contributions from cavity input and atomic polarization. The latter is modeled using the optical Bloch equations [3]. To arrive at Eq. (5), the intracavity field differential equation is time integrated from $-\infty$ to $+\infty$, at which times all fields are taken to be zero. The integration of the atomic polarization term is performed following Ref. [1]. In deriving Eq. (5) we also assumed that $\alpha L \ll 1$ and $\Delta \nu_{\text{inhom}} \gg 1/\tau_{\text{in}}$.

For a given θ_C^0, Eq. (5) describes the evolution of θ_C^{tot} as a function of $\eta = \alpha L/(1-R)$ and can be compared to the McCall-Hahn area theorem applicable to single-pass absorbers. Note that for $\eta/2 \gtrsim 1$, multiple values of θ_C^{tot} satisfy Eq. (5) for some ranges of θ_C^0. This effect has been pointed out previously in Ref. [17], where it is discussed in terms of optical bistability. It remains to be determined how the steady-state concept of bistability applies to the transient scenario under consideration, which evolves deterministically and therefore suggests single-valued mapping of inputs to outputs. We have performed numerical integration of the Maxwell-Bloch equations appropriate to the cavity + absorber system and compared results obtained with the analytic results of Eq. (5). We find that the numerically determined values of θ_C^{tot} coincide with the smallest θ_C^{tot} solution of Eq. (5) for a given θ_C^0. In what follows, values of θ_C^{tot} plotted represent the smallest solutions to Eq. (5) for a given θ_C^0.

In Fig. 2 we compare pulse-area evolution in the cavity (solid lines) and the SIT systems (dashed lines). For the cavity system, we plot θ_C^{tot} versus $\eta = \alpha L/(1-R)$ (left and upper axes). For the SIT system, we plot $\theta_{\text{out}}^{\text{SIT}}$ versus optical thickness αL (lower and right axes). Input-pulse areas correspond to the $\alpha L = \eta = 0$ values. Vertically adjacent values along the horizontal axes produce identical small signal attenuation.

In the cavity system, input areas less than π are seen to evolve continuously to zero for large η. This asymptotic be-
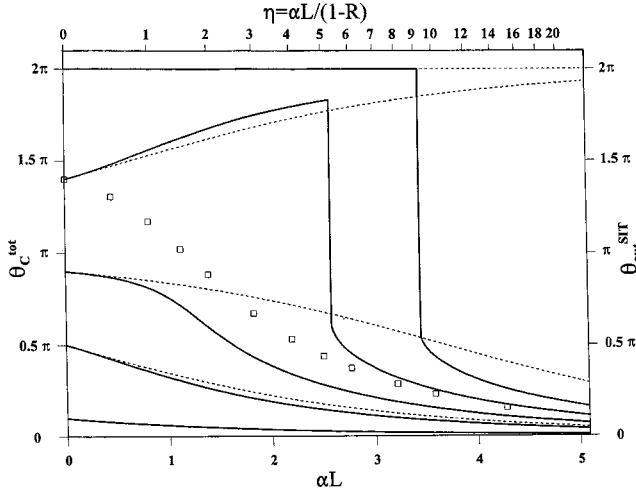
FIG. 2. Pulse area evolution for cavity and SIT systems. Solid lines, θ_C^{tot} vs $\eta = \alpha L/(1-R)$ (left and upper axes) for θ_C^0 values of 0.1π, 0.5π, 0.9π, 1.4π, 2π. Dashed lines, θ_{out}^{SIT} vs αL (right and lower axes). Squares, θ_{exc} vs η for $\theta_C^0 = 1.4\pi$. Vertically adjacent values along the horizontal axes produce identical small signal attenuation.

havior is familiar from the SIT system. Input areas satisfying $\pi < \theta_C^0 < 2\pi$ produce intracavity pulse areas θ_C^{tot} that initially approach 2π (again as in SIT), but suddenly drop toward zero at a θ_C^0 dependent critical value of η, i.e., η_c. Demanding $d\theta_C^0 / d\theta_C^{tot} = 0$ in Eq. (5) yields the θ_C^{tot} value immediately below the discontinuity

$$\theta_C^{tot} = \cos^{-1}\left(-\frac{\eta_c}{2}\right)^{-1}. \quad (6)$$

The critical value η_c at which the pulse area discontinuity occurs is obtained by inserting Eq. (6) into Eq. (5):

$$\theta_C^0 = \cos^{-1}\left(-\frac{\eta_c}{2}\right)^{-1} + \sqrt{\left(\frac{\eta_c}{2}\right)^2 - 1}. \quad (7)$$

Note that $\theta_C^{tot}(\theta_C^0 = 2\pi)$ remains stable at 2π until $\eta_c \approx 9$. The eventual instability of the 2π cavity solution at higher optical thickness contrasts with the complete stability of the 2π-SIT soliton.

The abrupt discontinuities in θ_C^{tot} seen in Fig. 2 are in sharp contrast to the behavior seen in the SIT system where output areas evolve to quantized values. The approach of θ_C^{tot} to analogous quantized values is frustrated by a dynamical instability in the underlying superradiant process, wherein the atomic emission behavior suddenly exhibits a dramatic change in character.

To shed further light on the dynamics underlying the area evolution of Fig. 2, we define the excitation pulse area θ_{exc}. θ_{exc} represents the intracavity pulse area accrued during the input-pulse duration τ_{in}, i.e., $\theta_{exc} = \theta_C(\tau_{in})$. We calculate θ_{exc} for $\theta_C^0 = 1.4\pi$ by numerically integrating the Maxwell-Bloch equations for the ring cavity shown in Fig. 1 and a temporally rectangular input pulse (rise/fall time 100 ns). We

plot θ_{exc} as the squares in Fig. 2. Increasing values of $\eta = \alpha L/(1-R)$ were realized by changing the optical thickness αL of the intracavity atoms from 0 to 0.3.

Recall that $\theta_{exc}(\theta_C^{tot})$ denotes the state of the line center atoms at $t = \tau_{in}$ $(t = \infty)$. At $\eta = 0$, the θ_{exc} and θ_C^{tot} values are equal. As η is increased, the difference between θ_{exc} and θ_C^{tot} grows and reveals the effect of postexcitation superradiance. The fact that $\theta_C^{tot} > \theta_{exc}$ indicates that superradiant atomic emission subsequent to the end of the input field drives line center atoms through an additional area. Remarkably, $\theta_C^{tot} > \theta_{exc}$ even where $\theta_{exc} < \pi$. Here, the line center atoms have not been completely inverted by the input field, yet continue to evolve to higher states of excitation, driven by superradiant emission that has the same phase as the input field and originates from atoms detuned from the absorption line center. Intriguingly, for $\eta < \eta_c$ and $\theta_{exc} < \pi$, the superradiant emission from detuned atoms completely inverts the line center atoms after which they continue to evolve back to the ground state. At $\eta = \eta_c$, θ_C^{tot} drops discontinuously to a value below π, indicating a very sudden nonlinearity in the resonant atom dynamics. Here, the superradiant emission generated by detuned atoms abruptly becomes insufficient to cause complete inversion of the resonant atoms.

It is interesting to further consider the cavity transmission characteristics for $\theta_C^0 = 2\pi$. Specifically, one might wonder whether the atom-cavity system permits lossless pulse transmission for this input area as is the case for the 2π-area solitons in the SIT system. We explore this issue numerically for the ring cavity shown in Fig. 1 with $R = 0.98$ and $\tau_c = 12$ ns. Again, $\Delta\nu_{inhom}$ was chosen to be large compared to both the excitation-field spectrum and cavity resonance, and the intracavity absorption αL was varied from 0 to 0.2. To quantify pulse energy loss we calculate the absorbed energy according to

$$E_{abs} = 1 - \frac{\int_0^\infty [P_r(t) + P_{out}(t)]dt}{\int_0^\infty P_{in}(t)dt}. \quad (8)$$

Here, P_{in}, P_r, and P_{out} are the powers of the input pulse, cavity reflection, and cavity output, respectively.

Figure 3 shows E_{abs} as a function of αL for excitation with 2-μs-long pulses of intracavity area $\theta_C^0 = 2\pi$ and various pulse shapes. The filled circles correspond to a hyperbolic-secant temporal pulse shape, the pulse shape leading to lossless propagation in SIT, the squares denote a temporally rectangular pulse. The solid line represents the pulse-shape-independent value of $\theta_C^{tot}(\alpha L)$, predicted by Eq. (5) with $R = 0.98$ and $\theta_C^0 = 2\pi$. The dashed-dotted line gives E_{abs} in the small-area limit, i.e., $\theta_C^0 \ll 1$.

Intriguingly, the energy fraction absorbed from the hyperbolic-secant pulse remains negligible up to $\alpha L \approx 0.04$, while the small-area absorption peaks at about 50% in the same regime. As αL is increased further, the pulse energy loss grows, while the total intracavity area θ_C^{tot} remains 2π. The initial energy loss is pulse-shape dependent, as is manifested in the different E_{abs}-versus-αL curve for the two pulse shapes. We conclude that the preservation of $\theta_C^{tot} = 2\pi$ over
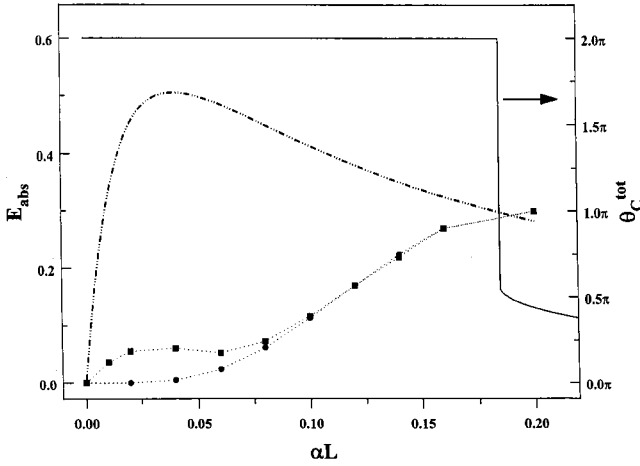
FIG. 3. Absorbed pulse energy vs intracavity absorption αL. Filled circles (squares), system excitation with a 2-μs-long pulse of $\theta_C^0 = 2\pi$ and a hyperbolic-secant (rectangular) pulse shape. Dash-dotted line, absorbed pulse energy in the small-area limit. Solid line, θ_C^{tot} for $\theta_C^0 = 2\pi$ as predicted by Eq. (5).

substantial ranges of αL does not generally imply lossless pulse transmission through the atom-cavity system. As shown in Fig. 3, the intracavity pulse area can maintain a constant value despite changing pulse energy content. This feature may provide a means to extract or add energy to a pulse without affecting its area.

Experimentally, two-mirror standing-wave cavities, with their longitudinal intensity variations, are easier to realize than traveling-wave cavities. It is possible to give an analytic area relationship for a two-mirror cavity (shown in Fig. 4):

$$\bar{\theta}_C^0 = \bar{\theta}_C^{\text{tot}}(\eta) + \eta J_1(2\bar{\theta}_C^{\text{tot}}(\eta)). \tag{9}$$

Here, J_1 denotes the Bessel function of the first kind, $\bar{\theta}_C^{\text{tot}}(\eta)$ is the total pulse area of either of the two counterpropagating traveling-wave components of the standing-wave intracavity field and $\bar{\theta}_C^0 = \bar{\theta}_C^{\text{tot}}(\eta=0)$ denotes the same parameter in the absence of atoms. In deriving Eq. (9) we took $R \approx 1$ in addition to the assumptions outlined in the derivation of Eq. (5). Figure 5 shows the functions $\theta_C^{\text{tot}}(\eta)$ predicted for the standing-wave cavity by Eq. (9) for various θ_C^0. Note that $\theta_C^{\text{tot}} = 2\bar{\theta}_C^{\text{tot}}$ is the total intracavity pulse area at an antinode of the standing-wave field. Interestingly, the behavior of the traveling and standing-wave cavities is similar except that the asymptotes to which θ_C^{tot} converges initially are shifted. Output areas are related to $\bar{\theta}_C^{\text{tot}}(\eta)$ by a constant factor.
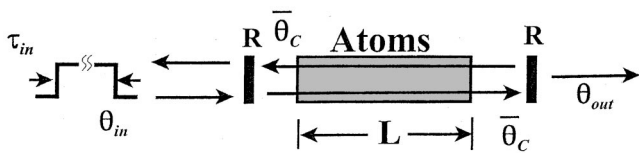
FIG. 4. Standing-wave cavity model system. $\bar{\theta}_C$, area of the counterpropagating traveling-wave fields. All other symbols as defined in Fig. 1.
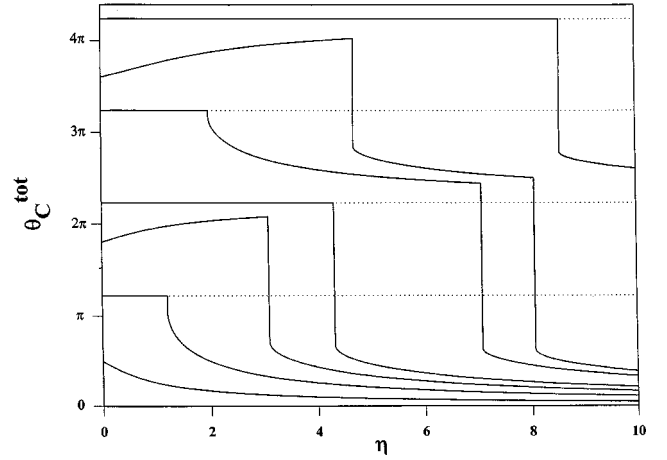
FIG. 5. θ_C^{tot} vs η for the standing-wave cavity for θ_C^0 values of 0.5π, 1.22π, 1.8π, 2.24π, 3.24π, 3.6π, and 4.24π.

To experimentally investigate the calculations presented above, we use the planospherical resonator shown in Fig. 6. Mirror M_1 (M_2) has a radius of curvature of $R_1 = \infty$ ($R_2 = 10$ cm). Both mirrors have a reflectivity $R = 0.98$ (± 0.01). The transverse cavity modes are nondegenerate. The free spectral range of the cavity is measured to be 11.3 GHz implying that the cavity's optical path length $L \approx 13.3$ mm. The minimum mode diameter ($1/e^2$ intensity points), located at M_1, is calculated to be $2\omega_0 = 185$ μm. The finesse and resonant transmission of the cavity, as measured outside the material absorption line, are $\mathcal{F} \approx 140$ and $T \approx 42\%$, respectively. Transmission less than unity indicates either incomplete coupling of the input light to the fundamental cavity mode, unequal mirror reflectivities, or a combination. The cavity's coherence time, deduced from the cavity linewidth, is $\tau_c \approx 2$ ns. A tubular piezoelectric actuator is sandwiched between the cavity mirrors. Cavity tuning in excess of one free spectral range at $T \approx 5$ K and ~ 800 nm was experimentally verified.

The sample employed is a 0.4-mm-long 0.25 at. % Tm^{3+}:YAG crystal. Both facets of the crystal are antireflection coated with specified reflectivity less than 0.1% at 793 nm. Tm^{3+} ions are excited on their $^3H_6(1) - ^3H_4(1)$ absorption line. At ~ 4.6 K, this transition has an inhomogeneous linewidth of ~ 20 GHz, a decoherence time T_2 of 20 μs, an excited state ($^3H_4$) lifetime T_1 of ~ 800 μs and a center wavelength $\lambda_{\text{air}} \approx 793.17$ nm. Tuning the cavity resonance within the inhomogeneously broadened absorption line al-
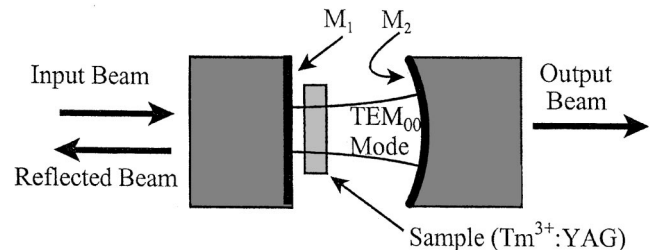
FIG. 6. Schematic of the experimental cavity and sample. M_1, cavity input mirror; M_2, cavity output mirror.
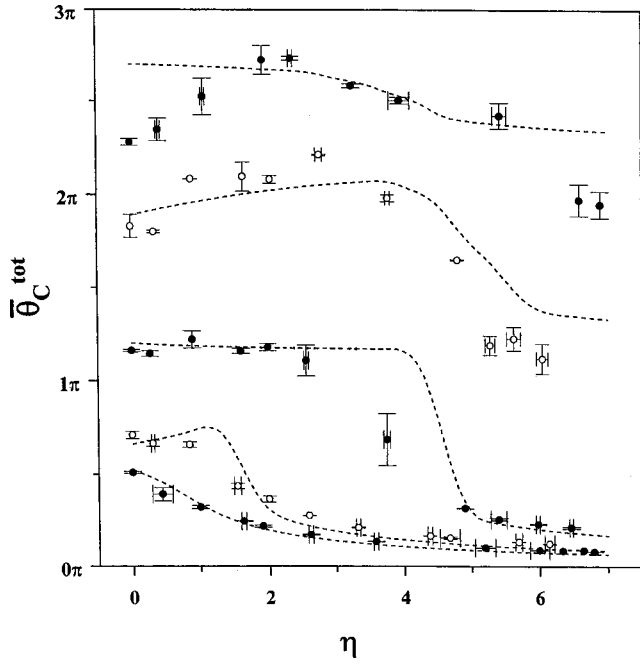
FIG. 7. $\overline{\theta}_C^{tot}$ vs η. Experimental data, circles. Dashed lines, theory. Data corresponding to the theory plots with θ_C^0 values of 0.5π, 1.2π, and 2.7π (0.65π, 1.9π) are represented as filled black (empty) circles.

lows access to single-pass sample absorptivities of 0–12%. The crystal is oriented such that the $\langle 110 \rangle$ direction coincides with the cavity's optical axis. The chosen crystal orientation combined with linearly polarized excitation pulses enables a single-valued ion-field coupling to the orientationally nonequivalent Tm^{3+} sites [18,19]. This situation was verified using a photon echo-diagnostic method. Cavity output signals were detected using a photodiode coupled to a transimpedance amplifier. The total detection bandwidth was 0–100 MHz.

In our experiments, the cavity output signal power, P_{out}, stimulated by a constant phase axial input field (a 2-μs-long rectangular pulse with rise/fall time $\sim$100 ns) is recorded. We estimate the beam-center-pulse area $\overline{\theta}_C^{tot}$ according to

$$\overline{\theta}_C^{tot} = \frac{2\pi\sqrt{2}a}{\sqrt{(1-R)\pi w_o^2}} \int P_{out}^{1/2} dt. \tag{10}$$

Here, $a = 56.6$ kHz cm/W$^{1/2}$ for light propagating along the $\langle 110 \rangle$ crystal direction with electric field polarization along $\langle 111 \rangle$ [19]. In writing Eq. (10), we assume, led by our numerical simulations, that the cavity output field has a constant phase.

Figure 7 shows the experimental values of $\overline{\theta}_C^{tot}$ versus η. Each data point shown represents an average over three individual excitation cycles with error bars denoting the standard deviation. η values depicted were obtained by dividing the measured single-pass optical thickness αL by the mirror transmission $1-R=0.02$. Different η values were realized

by tuning the cavity resonance to various spectral positions in the inhomogeneous absorption line. From bottom to top of Fig. 7, input powers of 0.06, 0.12, 0.27, 0.75, and 1.5 mW were employed.

The experimental input field exhibits a variation in transverse intensity. To compare constant-transverse-intensity theory with experiment, we divide the Gaussian transverse beam profile into annular sections of constant $\overline{\theta}_C^0$, weight them according to the fractional size of these sections and average the $\overline{\theta}_C^{tot}(\eta)$ functions obtained from the various regions. The total beam cross section over which we average in this manner contains about half of the total beam energy. The $\overline{\theta}_C^0$ values plotted correspond to beam-center values.

The experimental data clearly exhibits the principal features predicted by the theory of Fig. 5. Specifically, for $\overline{\theta}_C^0 = 0.5\pi$, the experiment reproduces the expected immediate monotonous fall of $\overline{\theta}_C^{tot}$ with η. For $\overline{\theta}_C^0 = 0.65\pi$ and $\overline{\theta}_C^0 = 1.2\pi$, the signature behavior of the area discontinuities, i.e., $\overline{\theta}_C^{tot} \approx \overline{\theta}_C^0$ initially, then subsequent fall to lower $\overline{\theta}_C^{tot}$ values approaching zero area for large η, is clearly manifest in the data. For $\overline{\theta}_C^0 = 1.9\pi$, the experimental area increases slightly with initial η values and then drops to lower θ_C^{tot} values, consistent with theory.

For $\overline{\theta}_C^0 = 1.2\pi$, the experimental area falls more gradually for $2.5 < \eta < 4.9$ than expected on the basis of Fig. 5. This disagreement between our model theory and experiment may follow from our simplistic modeling of transverse-intensity variation, i.e., assuming that atoms located at different transverse positions in the cavity mode evolve independently, or from the theoretical neglect of homogeneous dephasing, which is not entirely negligible over the experimental time scale. Detailed simulation for $\overline{\theta}_C^0 = 1.2\pi$ and $\eta \approx 4$, i.e., immediately to the left of the theoretically predicted area discontinuity, indicates that the atomic coherence longer than the experimentally available dephasing time is required for accurate measurement of the pulse area in this regime.

In conclusion, we have studied the pulse-area evolution in atom-cavity systems supporting cavity-accelerated superradiance for fixed input-pulse area when the effective optical thickness is increased. For low effective optical thickness the evolution of intracavity and output area is very similar to that predicted by McCall-Hahn for extended media. However, for higher effective optical thickness, discontinuous drops in output area occur that are unknown in the SIT system. Our experimental observations confirm the theoretical predictions. The area discontinuities may provide the basis for a "pulse-area switch," wherein the atom-cavity system is biased close to the area drop, and switching between two output areas occurs through modification of the effective optical thickness, e.g., by tuning the cavity resonance within the inhomogeneous absorption line. Such a device may be of interest in research areas where precise quantum state manipulation is important, e.g., quantum computing.

[1] S. L. McCall and E. L. Hahn, Phys. Rev. **183**, 457 (1969); Phys. Rev. Lett. **18**, 908 (1967).

[2] G. L. Lamb, Jr., Rev. Mod. Phys. **43**, 99 (1971).

[3] L. Allen and J. H. Eberly, *Optical Resonance and Two-Level Atoms* (Dover, New York, 1978); A. I. Maimistov, A. M. Basharov, S. O. Elyutin, and Yu. M. Sklyarov, Phys. Rep. **191**, 1 (1990).

[4] C. K. N. Patel and R. E. Slusher, Phys. Rev. Lett. **19**, 1019 (1967); C. K. Rhodes, A. Szöke, and A. Javan, *ibid.* **21**, 1151 (1968); C. K. N. Patel, Phys. Rev. A **1**, 979 (1970); F. A. Hopf, C. K. Rhodes, and A. Szöke, Phys. Rev. B **1**, 2833 (1970); P. K. Cheo and C. H. Wang, Phys. Rev. A **1**, 225 (1970); I. M. Asher, Phys. Rev. A **5**, 349 (1972); I. M. Asher and M. O. Scully, Opt. Commun. **3**, 395 (1971); H. M. Gibbs and R. E. Slusher, Phys. Rev. A **6**, 2236 (1972).

[5] R. E. Slusher and H. M. Gibbs, Phys. Rev. A **5**, 1634 (1972); **6**, 1255 (1972).

[6] H. P. Grieneisen, J. Goldhar, N. A. Kurnit, A. Javan, and H. R. Schlossberg, Appl. Phys. Lett. **21**, 559 (1972).

[7] H. M. Gibbs and R. E. Slusher, Appl. Phys. Lett. **18**, 505 (1971).

[8] A. Rahman, Phys. Rev. A **60**, 4187 (1999); A. Rahman and J. H. Eberly, Opt. Express **4**, 133 (1999).

[9] A. Guzman, F. S. Locati, M. Romagnoli, and S. Wabnitz, Phys. Rev. A **46**, 1594 (1992); A. Guzman, M. Romagnoli, and S. Wabnitz, Appl. Phys. Lett. **56**, 614 (1990).

[10] J. H. Eberly, Opt. Express **2**, 173 (1998).

[11] C. Greiner, B. Boggs, and T. W. Mossberg, Phys. Rev. Lett. **85**, 3793 (2000).

[12] Reviews on superradiance can be found in M. S. Feld and J. C. MacGillivray, in *Coherent Nonlinear Optics*, edited by M. S. Feld and V. S. Letokokv (Springer, Berlin, 1980), p. 7; Q. H. F. Vrehen and H. M. Gibbs, in *Dissipative Systems in Quantum Optics*, edited by R. Bonifacio, Springer Topics in Current Physics 21 (Springer, Berlin, 1982), p. 111; M. G. Benedict, A. M. Ermoloaev, V. A. Malyshev, I. V. Sokolov, and E. D. Trifonov, *Superradiance: Multiatomic Coherent Emission* (Institute of Physics Publishing, Bristol, 1996).

[13] N. Skribanowitz, I. P. Herman, J. C. MacGillivray, and M. S. Feld, Phys. Rev. Lett. **30**, 309 (1973); M. Gross, C. Fabre, P. Pillet, and S. Haroche, *ibid.* **36**, 1035 (1976); A. Flusberg, T. Mossberg, and S. R. Hartmann, Phys. Lett. **58A**, 373 (1976); H. M. Gibbs, Q. H. F. Vrehen, and H. M. J. Hikspoors, Phys. Rev. Lett. **39**, 547 (1977).

[14] N. E. Rehler and J. E. Eberly, Phys. Rev. A **3**, 1735 (1971); R. Bonifacio, P. Schwendimann, and F. Haake, *ibid.* **4**, 302, 854 (1971); R. Bonifacio and L. A. Lugiato, *ibid.* **11**, 1507 (1975).

[15] R. H. Dicke, Phys. Rev. **93**, 99 (1954).

[16] C. Greiner, T. Wang, T. Loftus, and T. W. Mossberg, Phys. Rev. Lett. **87**, 253602 (2001).

[17] S. M. Zakharov, Zh. Eksp. Teor. Fiz. **108**, 829 (1995) [JETP **81**, 452 (1995)].

[18] C. Greiner, B. Boggs, T. Loftus, T. Wang, and T. W. Mossberg, Phys. Rev. A **60**, R2657 (1999).

[19] Y. Sun, G. M. Wang, R. L. Cone, R. W. Equall, and M. J. M. Leask, Phys. Rev. B **62**, 15443 (2000).